Compressed Optoacoustic Sensing of Volumetric Cardiac Motion

Ali Özbek, Xosé Luís Deán-Ben, and Daniel Razansky, *Member, IEEE*

***Abstract*— The recently developed optoacoustic tomography systems have attained volumetric frame rates exceeding 100 Hz, thus opening up new venues for studying previously invisible biological dynamics. Further gains in temporal resolution can potentially be achieved via partial data acquisition, though a priori knowledge on the acquired data is essential for rendering accurate reconstructions using compressed sensing approaches. In this work, we suggest a machine learning method based on principal component analysis for high-frame-rate volumetric cardiac imaging using only a few tomographic optoacoustic projections. The method is particularly effective for discerning periodic motion, as demonstrated herein by non-invasive imaging of a beating mouse heart. A training phase enables efficiently compressing the heart motion information, which is subsequently used as prior information for image reconstruction from sparse sampling at a higher frame rate. It is shown that image quality is preserved with a 64-fold reduction in the data flow. We demonstrate that, under certain conditions, the volumetric motion could effectively be captured by relying on time-resolved data from a single optoacoustic detector. Feasibility of capturing transient (non-periodic) events not registered in the training phase is further demonstrated by visualizing perfusion of a contrast agent in vivo. The suggested approach can be used to significantly boost the temporal resolution of optoacoustic imaging and facilitate development of more affordable and data efficient systems.**

***Index Terms*— Image acquisition, image reconstruction, image restoration, machine learning, optoacoustic imaging.**

I. Introduction

VISUALIZATION of rapid biological dynamics is often hampered with the existing imaging modalities due to the need for sequential acquisition of tomographic data, which limits the achievable temporal resolution, in particular when it comes to volumetric (3D) imaging. In contrast, it only takes a single nanosecond-duration laser pulse to generate a full tomographic dataset in optoacoustic imaging, both in 2D [1], [2] and 3D [3], [4]. This enables effectively "freezing" the tissue motion and imaging at frame rates ultimately limited by the unidirectional propagation of ultrasound through the region of interest (ROI). State-of-the-art volumetric optoacoustic tomography (VOT) systems based on simultaneous acquisition of 512 signals (projections) have enabled the visualization of very fast biological processes, such as cardiovascular dynamics or neuronal activity, at 3D frame rates of 100 Hz [5], [6].

In practice, the temporal resolution of optoacoustic imaging is effectively constrained by the data throughput capacity of imaging systems. One way to accelerate the achievable frame rate consists in partial (sparse) sampling of tomographic data for each laser pulse [7], [8]. The missing information can then be recovered by considering prior knowledge on the acquired data. For example, compressed sensing (CS) schemes achieve this by assuming that the signals (or images) are sparse in a certain domain, i.e. the data to be recovered exhibits low entropy. Such approaches have recently attracted great attention as they enabled full recovery of the reconstructed image quality from sparse signals sampled below the Nyquist rate [9], [10]. CS has further been successfully exploited for tomographic reconstructions from sparse data in several 2D and 3D optoacoustic embodiments [8], [11], [12], thus enabling imaging of freely swimming fish embryos at kilohertz volumetric frame rates [12]. To this end, several systems providing 4D (real-time 3D) optoacoustic imaging capabilities have been reported [13]–[18]. The frame rate is typically limited by the data throughput capacity, which can potentially be significantly accelerated by devising efficient data compression strategies.

The main limitations of CS-based methods often stem from the lack of accurate a priori knowledge on the data sparsity.

Manuscript received January 8, 2020; revised March 6, 2020; accepted March 11, 2020. Date of publication May 28, 2020; date of current version September 30, 2020. This work was supported in part by the European Research Council under Agreement ERC-2015-CoG-682379. The work of Xosé Luís Deán-Ben was supported by the Werner and Hedy Berger-Janser Foundation (application No 8/2019). *(Corresponding author: Ali Özbek.)*

Ali Özbek is with the Institute for Biomedical Engineering, ETH Zürich, 8092 Zürich, Switzerland, also with the Department of Information Technology and Electrical Engineering, ETH Zürich, 8092 Zürich, Switzerland, and also with the Institute for Biological and Medical Imaging, Helmholtz Center Munich, 85764 Oberschleißheim, Germany (e-mail: oezbeka@student.ethz.ch).

Xosé Luís Deán-Ben is with the Faculty of Medicine, University of Zurich, 8006 Zürich, Switzerland, also with the Institute of Pharmacology and Toxicology, University of Zurich, 8006 Zürich, Switzerland, also with the Institute for Biomedical Engineering, ETH Zurich and University of Zurich, 8092 Zürich, Switzerland, and also with the Department of Information Technology and Electrical Engineering, ETH Zürich, 8092 Zürich, Switzerland (e-mail: xl.deanben@pharma.uzh.ch).

Daniel Razansky is with the Faculty of Medicine, University of Zurich, 8006 Zürich, Switzerland, also with the Institute of Pharmacology and Toxicology, University of Zurich, 8006 Zürich, Switzerland, also with the Institute for Biomedical Engineering, ETH Zurich and University of Zurich, 8092 Zürich, Switzerland, also with the Department of Information Technology and Electrical Engineering, ETH Zürich, 8092 Zürich, Switzerland, and the Institute for Biological and Medical Imaging, Helmholtz Center Munich, 85764 Oberschleißheim, Germany (e-mail: daniel.razansky@uzh.ch).

This article has supplementary downloadable material available at http://ieeexplore.ieee.org, provided by the authors.

Color versions of one or more of the figures in this article are available online at http://ieeexplore.ieee.org.

Digital Object Identifier 10.1109/TMI.2020.2985134

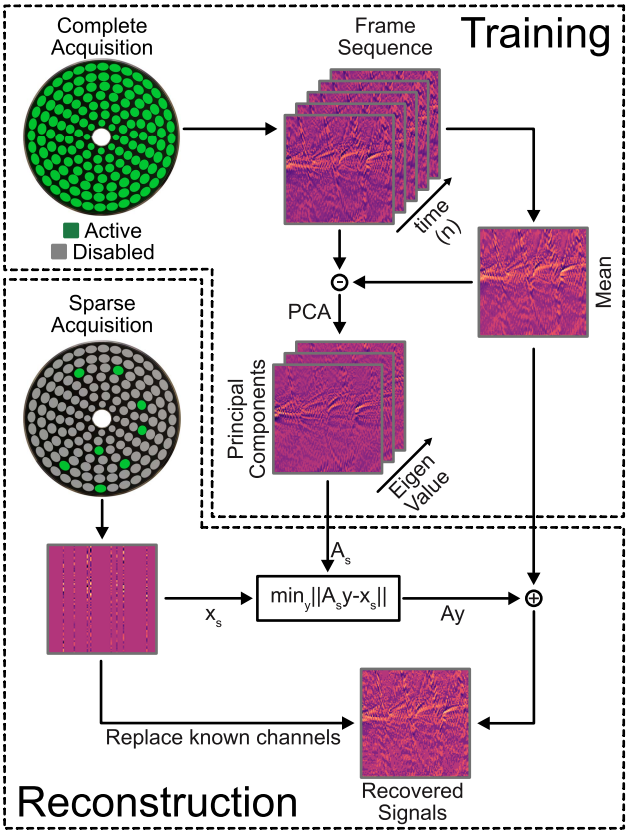

Fig. 1. Data acquisition and image reconstruction protocol of the PCA-based method. The training phase (top section) involves acquiring optoacoustic data with all the available channels and subsequent processing to extract the principal components from the image sequence. Reconstruction phase (bottom section) involves acquisition of signals from fewer channels. Image quality recovery for the subsampled data is achieved by means of the previously learned principal components.

In principle, prior information can be obtained by training machine learning algorithms on the specific type of acquired data [19]–[22]. In this work, we suggest a machine learning method based on principal component analysis (PCA) for optimization and acceleration of the data acquisition protocol for cardiac optoacoustic imaging. PCA is based on reducing the dimensionality of a large number of random variables by analyzing their mutual correlations. Thereby, it is particularly suitable for compressing periodic heartbeat data with a high degree of correlation between the motion of different voxels.

II. Methods

A. Algorithm

The PCA protocol is schematically illustrated in Fig. 1. The training phase was performed with datasets consisting of 300 frames with sets of $n_{ch} = 512$ time resolved signals with $n_{ch} = 494$ samples (required to effectively cover the field of view). The captured signals were subsampled to a lower frame rate from the original 100 Hz dataset. The subsampled signal samples, after subtraction of the inter-frame average (DC) component, were considered as a data matrix $\boldsymbol{X} \in \mathbb{R}^{M\times N}$ of $N = n_{ch}n_s$ possibly correlated variables. Each of the frames is considered as an observation of such row vector $p \in \mathbb{R}^N$ whereas, each variable represents a single pixel of the signal matrix. Note that signals from different channels are concatenated to form p. High correlation of the variables in vector $\boldsymbol{X}$ is associated with similarities in temporal variations of the signal samples (time domain sparsity) and is not related to the potential spatial domain sparsity of the object that generated such signals. The PCA transformation renders a set of $n-1$ principal components, calculated from the eigen-decomposition of the covariance matrix $\boldsymbol{Q}$ defined as

$$\boldsymbol{Q} = \frac{1}{n-1}\boldsymbol{X}^T\boldsymbol{X}, \tag{1}$$

being $\boldsymbol{X}$ a matrix whose columns contain the n observations of $\boldsymbol{X}$. The eigenvectors of $\boldsymbol{Q}$ form a transformation matrix $\boldsymbol{A} \in \mathbb{R}^{N\times K}$ with N variables and $K = n-1$ principal components, which corresponds to $\sim$ 283MiB of training data. Note that image quality can potentially be improved by selecting K to be below $n-1$, which is further investigated in section III. The matrix transforms a vector from the principal component space into the signal space. The PCA protocol is aimed at recovering the missing time-resolved signals. After this step, any reconstruction algorithm can be employed to render the 3D images. The training phase allows "learning" a matrix $\boldsymbol{A}$ of principal component coefficients to be used for the reconstruction of the entire signal sequence from sparse (subsampled) data. In this reconstruction phase, a vector $x_s \in \mathbb{R}^{n_{chs}\times n_s}$ corresponding to sparse spatial sampling from only a few sensors (channels) was considered, where n_{chs} is the number of channels in the subsampled data. For each sparse acquisition, the projection of the entire frame along the principal component directions $w \in \mathbb{R}^K$ was estimated as solution of an inverse problem defined as

$$w = \underset{y}{argmin}\,||\boldsymbol{A_s}y - x_s||, \tag{2}$$

and calculated via

$$w = \boldsymbol{A}_s^{+}x_s, \tag{3}$$

where $\boldsymbol{A}_s$ is a matrix obtained from $\boldsymbol{A}$ by removing the rows corresponding to missing channels in the subsampled data and $\boldsymbol{A}_s^{+}$ is its pseudo-inverse. w was subsequently projected along the p directions corresponding to all samples as

$$x = \boldsymbol{A}w'. \tag{4}$$

No sparsity condition (e.g. l^1 regularization) needs to be imposed for inverting the principal component matrix in (2). In PCA decomposition, the components are ordered according to their contribution to the image i.e. the eigenvalues. By limiting the number of principal components used during the inversion, a constraint is effectively imposed that reduces likelihood of overfitting. The recovered frame was eventually obtained by adding the previously calculated average of the training frames and substituting the already present channels in the subsampled dataset. Both training and recovery phases are solely accomplished in the signal domain without the need for image reconstruction. This enables faster and more memory efficient calculations.

B. Experimental Measurements

The VOT system used for acquisition of the 4D data consists of a custom-made piezo-composite spherical array transducer

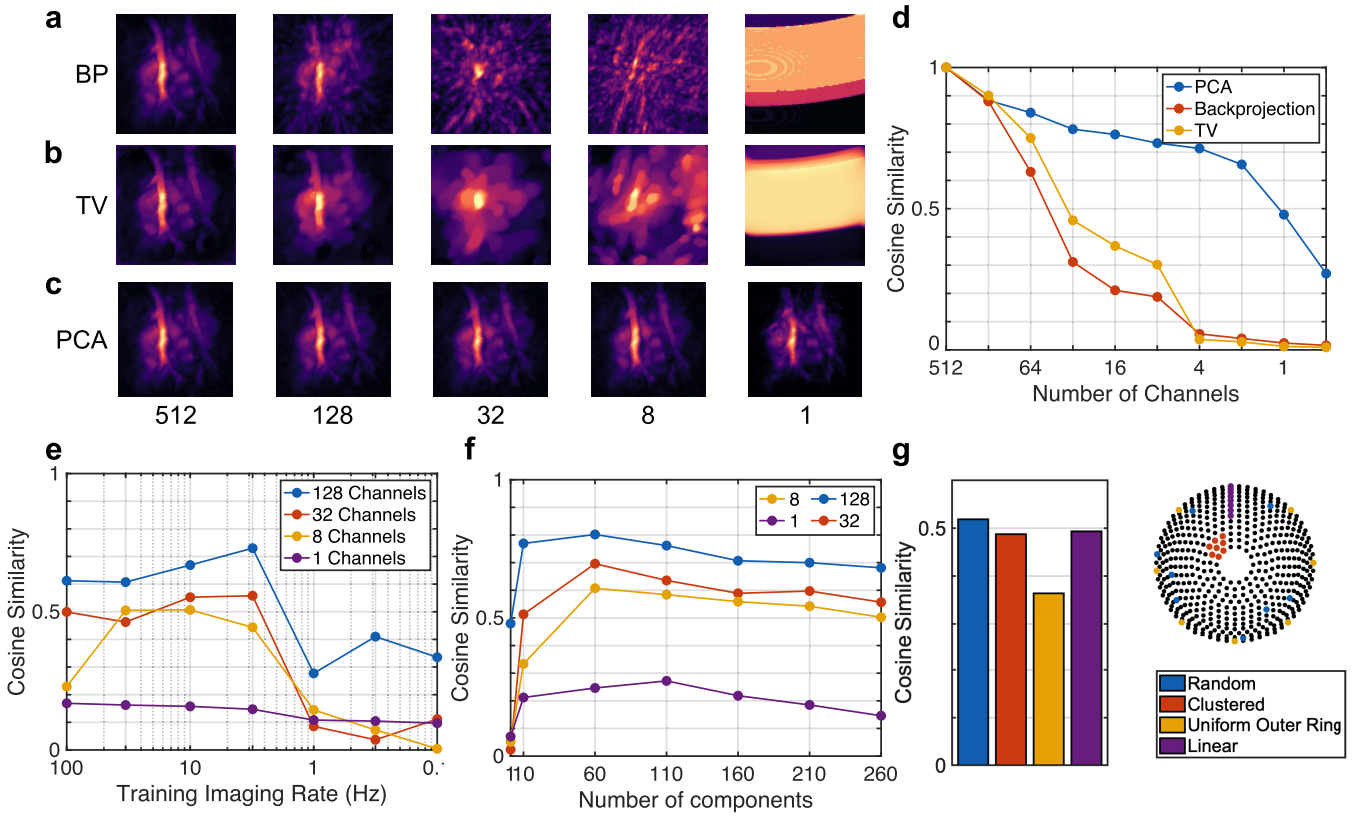

Fig. 2. Quality comparison between conventional and PCA-recovered reconstructions. (a) Images rendered with the conventional back-projection (BP) algorithm when reducing the number of acquired channels (indicated in each column). (b) The corresponding images reconstructed with a model-based algorithm including a total variation regularization term. (c) The corresponding images reconstructed with BP after signal recovery with the PCA-based approach. (d) Cosine similarity between the ground-truth (first column in panel a) and other reconstructions as a function of the number of simultaneously acquired channels. Cosine similarity between the ground-truth and PCA as a function of various training frame rates (e) and number of principal components (f) for reconstructions with various subsampling factors. (g) Comparison of cosine similarity to ground truth for various spatial detector distributions, as indicated with the corresponding colors in the schematic array representation.

(Imasonic SaS, Voray, France) featuring 512 individual circular elements with 2.5 mm diameter, 5 MHz central detection frequency and $\sim$ 80% bandwidth. The spherical detection surface of the array has a radius of 40 mm and 140° angular coverage (1.3π solid angle), providing nearly isotropic spatial resolution of 150 μm at its center [23]. Optoacoustic data was acquired by exciting the tissue with a short-pulsed (<10 ns) laser tuned to a wavelength of 800 nm and operating at a pulse repetition frequency (PRF) of 100 Hz. All signals from the transducer elements were simultaneously digitized with a custom-made data acquisition system (DAQ, Falkenstein Mikrosysteme GmbH, Taufkirchen, Germany) capable of digitizing 494 samples at 40 megasamples per second from 512 channels simultaneously.

Performance of the suggested PCA approach was tested by non-invasive imaging of the heart in hairless NOD.SCID mice (Envigo, Rossdorf, Germany). For imaging, the mouse was placed in supine position on top of an agar block filling the volume between the animal and active surface of the transducer array. Ultrasound gel was further applied to ensure acoustic coupling between the skin and the agar medium. During the measurements, the mouse was anesthetized using a $\sim$ 2% isoflurane-medical air mixture ($\sim$ 0.8 l/min gas flow). The energy density per pulse at the surface of the mouse was approximately 12 mJ/cm, below safety standards for laser exposure. All animal experiments were performed in full compliance with institutional guidelines and with approval from the Government of Upper Bavaria.

Prior to PCA processing, all signals recorded by the DAQ were filtered by a finite impulse response filter with cut-off frequencies of 0.5-8 MHz and deconvolved with the impulse response of the transducer elements. As previously described, the training was performed by considering 300 out of the 3000 original frames, i.e. operating at 10 Hz effective imaging frame rate, which is a common pulse repetition rate of flash-lamp-pumped lasers ensuring an optimal trade-off between signal-to-noise and safe laser exposure levels [24]. However, we further evaluated how subsampling at other frame rates affects the resulting image quality. Due to the instantaneous excitation of optoacoustic responses across the entire organ, all samples from the individual optoacoustic waveforms (projections) correspond to the same phase of the cardiac cycle. Although irregular movements originating from e.g. breathing or arrhythmic events may lead to distortions, the spatio-temporal information is generally expected to be encoded in a few principal components. After training, a set of 1500 frames (different from the training set) at the original frame rate of 100 Hz was reconstructed. Sparse acquisition was simulated

by considering a reduced number of channels, whereas data from all the 512 channels was taken as reference. Tomographic reconstructions of both the recovered and reference frames were performed with a filtered 3D back-projection formula [25] implemented on a graphics processing unit (NVIDIA GeForce GTX TITAN X). The training phase of the algorithm (calculation of the transformation matrix) with 300 frames was accomplished within approximately 6.3 s. Recovery of each image frame has taken on average 5.4 ms. Both phases of the algorithm are running on an Intel i7-7700K CPU with 64 GB of RAM. When employing GPU-accelerated backprojection reconstruction [26], each frame containing 100×100x100 voxels can be recovered from the undersampled data within less than 33 ms, thus allowing for real-time image rendering and preview.

III. Results

As expected, both the PCA-recovered frames and their unprocessed equivalents yield equally good results when data from all the channels are used for the reconstruction. However, quality of the images reconstructed from sparse data using the conventional 3D back-projection algorithm deteriorates significantly when reducing the number of channels (Fig. 2a). Similar deterioration was observed when using a more advanced model-based algorithm imposing a spatial sparsity condition via the total variation (TV) regularization term (Fig. 2b). On the other hand, the image quality is largely preserved with the suggested PCA-based processing, even when only employing data from a single channel for the reconstructions (Fig. 2b). A more quantitative comparison is provided in Fig. 2d, which displays the cosine similarity metric between the three reconstruction strategies calculated via

$$\frac{a \cdot b}{||a||||b||} \tag{5}$$

where a and b are vectors representing two images and $||\cdot||$ is the l^2-norm.

Similarity between images reconstructed from the sub- and fully-sampled data was calculated for an image sequence corresponding to a time interval of 1 second (roughly 5 heart cycles). The mean image was subtracted before calculating the cosine similarity in order to compare the methods' accuracy in the presence of temporal variations while discarding the static component of the image sequence. Clearly, features of the original image are better preserved when PCA processing is employed, particularly when reconstructing from less than 128 channels (Fig. 2d). The PCA-based method is further capable of maintaining accuracy over a large range of training frame rates (Fig. 2e) whereas significant image quality deterioration only starts at 3 Hz (>30 subsampling factor). Dependence of the reconstruction quality, similarly estimated via the cosine similarity, on the number of principal components is presented in Fig. 2f. Indeed, the PCA method can recover the missing data even from a few principal components. A slight decline in the image accuracy can be observed with increasing number of principal components, which can be ascribed to overfitting. In fact, distribution of the active elements plays an important role in establishing the reconstructed image quality

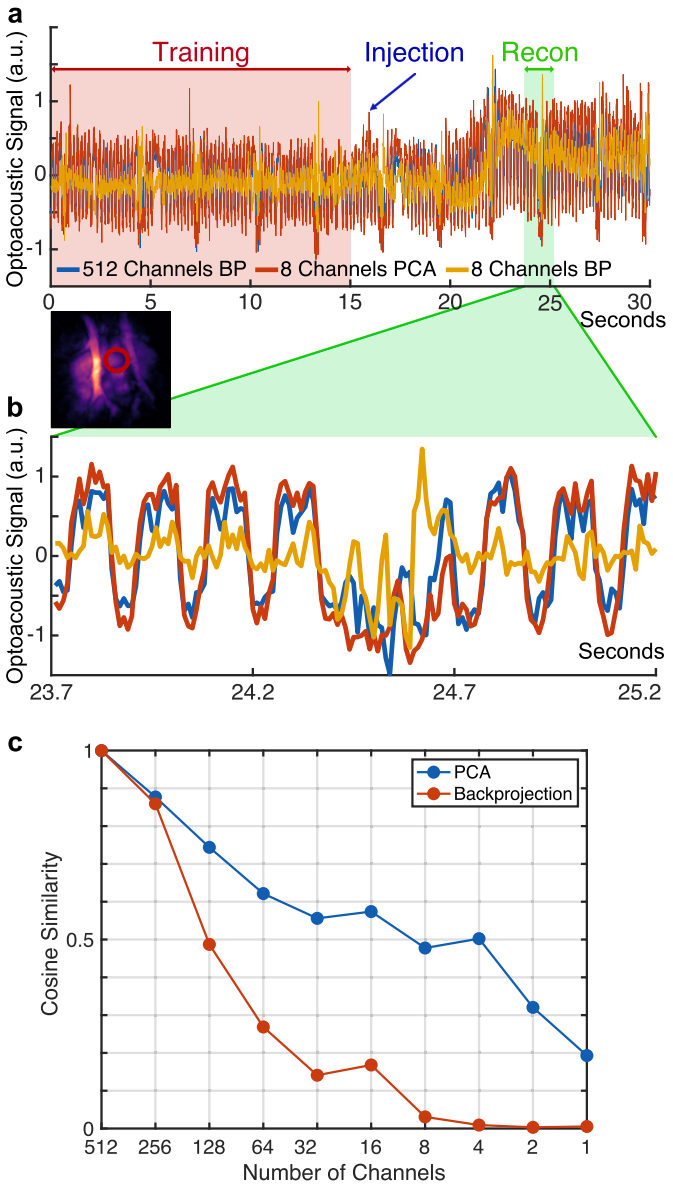

Fig. 3. Data acquisition and image reconstruction protocol of the PCA-based method. The training phase (a) involves acquiring optoacoustic data with all the available channels and subsequent processing to extract the principal components from the image sequence. Reconstruction phase (b) involves acquisition of signals from fewer channels. Image quality recovery for the subsampled data is achieved by means of the previously learned principal components (c).

(Fig. 2g) whereas the highest cosine similarity corresponds to a random distribution of elements. The other configurations had comparable performance except for the uniform outer ring distribution, arguably due to the strong signals generated by the heart surface. Those are chiefly propagating perpendicular to the skin hence not efficiently collected by the elements located on the outer ring.

The method's robustness in identifying transient events not originally present in the training phase was subsequently tested by injecting 100 ml (100 nmol) of indocyanine green (ICG) through the tail vein of the mouse. 3000 frames were acquired at 100 Hz, whereas the injection was done 16 s after commencement of the signal acquisition. Training was performed

with the first 150 out of 1500 fully-sampled frames (temporally downsampled to 10 Hz) corresponding to the first 15 s of the recording (Fig. 3a), while the remaining frames were subsequently reconstructed with only 8 randomly- selected channels. The signal increase corresponding to the appearance of the ICG bolus can clearly be discerned around 20-25 s after the beginning of the acquisition by observing a representative voxel intensity from the reconstructed image sequence. Fig. 3b displays a more detailed comparison of the different profiles in a narrower time window containing several cardiac cycles and one irregular motion event presumably related to breathing. A more quantitative comparison is presented in Fig. 3c, where the cosine similarity between the ground truth and both methods are shown as a function of number of channels used for reconstruction. The similarity was calculated for a time window between 20 and 25 seconds after the start of the acquisition. This time window covers the image intensity increase due to ICG injection as well as a breathing event. It is shown that the PCA method was able to follow the temporal signal changes much more reliably than the standard back projection reconstruction applied to the sparse data. The results further indicate that the PCA-processed time profiles of the sparsely reconstructed data accurately follow the reference profiles, whereas the time profiles from the unprocessed images remain largely distorted. A visual comparison between the different reconstruction approaches is provided in Supplementary Video 1 available in the online version of the journal.

IV. Discussion and Conclusions

The presented results demonstrate the feasibility of a highly compressed acquisition of volumetric optoacoustic data in the presence of periodic motion. Training of the PCA-based algorithm with densely sampled 512-channel data recorded at 10 Hz has enabled here high quality imaging at a rate of 100 Hz using just a small fraction of the channels. In fact, the proposed method was capable of rendering real-time volumetric images of the mouse heart with 1/64th of the channels without substantial impact on the image quality and even operated reasonably well under single channel acquisition conditions. In principle, the first eigenvector obtained from the PCA analysis is sufficient to describe a sequence of images featuring a synchronous periodic motion. Note that the heart motion is not fully synchronized for all the image voxels while it is further superimposed by breathing motion occurring at a different frequency. Accurate reconstructions could yet be obtained with relatively low number of eigenvectors, evincing data compression efficiency of the suggested approach. The relatively short (sub-minute) training times and real-time image rendering may further enable dynamic alteration of the experimental parameters based on real-time image feedback. Furthermore, the developed PCA-based method can be equally applied to arbitrary laser pulse repetition and imaging frame rates also beyond 100 Hz.

It has been previously demonstrated that compressed acquisition of tomographic optoacoustic data can alternatively be facilitated by encoding spatial data into temporal domain signatures [27], [28]. However, such solutions necessitated additional hardware, e.g. scanning of the excitation laser beam, employing ergodic relays or adding randomly distributed scatterers around the imaged object. Furthermore, computationally costly models based upon non-differentiable inversion methods are required to generate images with those methods. In contrast, the method proposed herein can be used without altering the experimental setup. Following signal recovery, a simple back-projection reconstruction can then be used to render images in real-time.

The PCA-guided reconstruction of sparsely acquired data is not restricted to periodic motion and can accurately recover dynamic events that were not part of the training phase. This was demonstrated here by volumetric tracking of contrast agent perfusion but other transient events can potentially be recovered, such as cardiac arrhythmias. Note that the ICG injection was performed at a relatively slow rate in our experiments and hence imaging of faster transient events may not be possible or require additional training. Unlike other compressed sensing methods relying on spatial sparsity, the suggested PCA-based method efficiently exploits the temporal sparsity of the data while preserving well spatial features of the images. The suggested approach is not of sole relevance to cardiac imaging and may potentially be applied to other biological data containing strong periodic component, e.g. stimulus-evoked brain responses. In general, VOT has significance for neuroimaging applications as it is sensitive to both label-free hemodynamic responses [29], [30] as well as calcium or voltage labels that represent neural activity more directly [31], [32].

The low degree of spatial domain sparsity in the heart images indicates that the suggested approach can outperform generalized CS algorithms commonly based on adding a l^1 regularization term to the reconstruction procedure (e.g. to the gradient or the wavelet transform of the image). CS may have a better performance for imaging fast transient events when sparsity conditions apply. However, PCA may potentially serve for the same purpose if proper training is performed. Furthermore, the method can be improved to better account for translation and scaling of the image data to allow for broader applicability. In conclusion, the suggested machine learning approach based on PCA can be used to significantly boost the temporal resolution of volumetric optoacoustic imaging and facilitate development of more affordable and data efficient systems.

References

[1] L. Ding, X. L. Deán-Ben, and D. Razansky, "Real-time model-based inversion in cross-sectional optoacoustic tomography," *IEEE Trans. Med. Imag.*, vol. 35, no. 8, pp. 1883–1891, Aug. 2016.

[2] A. Buehler, M. Kacprowicz, A. Taruttis, and V. Ntziachristos, "Real-time handheld multispectral optoacoustic imaging," *Opt. Lett.*, vol. 38, no. 9, pp. 1883–1891, 2016.

[3] X. L. Deán-Ben, S. J. Ford, and D. Razansky, "High-frame rate four dimensional optoacoustic tomography enables visualization of cardiovascular dynamics and mouse heart perfusion," *Sci. Rep.*, vol. 5, no. 1, Sep. 2015, Art. no. 10133.

[4] S. Gottschalk, T. F. Fehm, X. L. Deán-Ben, V. Tsytsarev, and D. Razansky, "Correlation between volumetric oxygenation responses and electrophysiology identifies deep thalamocortical activity during epileptic seizures," *Neurophotonics*, vol. 4, no. 1, Oct. 2016, Art. no. 011007.

[5] H.-C.-A. Lin *et al.*, "Ultrafast volumetric optoacoustic imaging of whole isolated beating mouse heart," *Sci. Rep.*, vol. 8, no. 1, Dec. 2018, Art. no. 14132.

[6] S. Gottschalk, T. F. Fehm, X. L. Deán-Ben, and D. Razansky, "Noninvasive real-time visualization of multiple cerebral hemodynamic parameters in whole mouse brains using five-dimensional optoacoustic tomography," *J. Cerebral Blood Flow Metabolism*, vol. 35, no. 4, pp. 531–535, Apr. 2015.

[7] C. G. Graff and E. Y. Sidky, "Compressive sensing in medical imaging," *Appl. Opt.*, vol. 54, no. 8, pp. C23–C44, 2015.

[8] Z. Guo, C. Li, L. Song, and L. V. Wang, "Compressed sensing in photoacoustic tomography *in vivo*," *J. Biomed. Opt.*, vol. 15, no. 2, 2010, Art. no. 021311.

[9] D. L. Donoho, "Compressed sensing," *IEEE Trans. Inf. Theory*, vol. 52, no. 4, pp. 1289–1306, Apr. 2006.

[10] E. J. Candes, J. Romberg, and T. Tao, "Robust uncertainty principles: Exact signal reconstruction from highly incomplete frequency information," *IEEE Trans. Inf. Theory*, vol. 52, no. 2, pp. 489–509, Feb. 2006.

[11] S. Arridge *et al.*, "Accelerated high-resolution photoacoustic tomography via compressed sensing," *Phys. Med. Biol.*, vol. 61, no. 24, pp. 8908–8940, Dec. 2016.

[12] A. Özbek, X. L. Deán-Ben, and D. Razansky, "Optoacoustic imaging at kilohertz volumetric frame rates," *Optica*, vol. 5, no. 7, pp. 857–863, Jul. 2018.

[13] L. Xiang, B. Wang, L. Ji, and H. Jiang, "4-D photoacoustic tomography," *Sci. Rep.*, vol. 3, no. 1, Dec. 2013, Art. no. 1113.

[14] T. F. Fehm, X. L. Deán-Ben, and D. Razansky, "Four dimensional hybrid ultrasound and optoacoustic imaging via passive element optical excitation in a hand-held probe," *Appl. Phys. Lett.*, vol. 105, no. 17, Oct. 2014, Art. no. 173505.

[15] A. Taruttis and V. Ntziachristos, "Advances in real-time multispectral optoacoustic imaging and its applications," *Nature Photon.*, vol. 9, no. 4, p. 219, 2015.

[16] Y. Matsumoto *et al.*, "Label-free photoacoustic imaging of human palmar vessels: A structural morphological analysis," *Sci. Rep.*, vol. 8, no. 1, Dec. 2018, Art. no. 786.

[17] X. L. Deán-Ben, H. López-Schier, and D. Razansky, "Optoacoustic micro-tomography at 100 volumes per second," *Sci. Rep.*, vol. 7, no. 1, Dec. 2017, Art. no. 6850.

[18] F. Lucka *et al.*, "Enhancing compressed sensing 4D photoacoustic tomography by simultaneous motion estimation," *SIAM J. Imag. Sci.*, vol. 11, no. 4, pp. 2224–2253, Jan. 2018.

[19] D. Lee, J. Yoo, and J. C. Ye, "Deep residual learning for compressed sensing MRI," in *Proc. IEEE 14th Int. Symp. Biomed. Imag. (ISBI)*, Apr. 2017, pp. 15–18.

[20] A. Hauptmann *et al.*, "Approximate k-space models and deep learning for fast photoacoustic reconstruction," in *Proc. Int. Workshop Mach. Learn. Med. Image Reconstruction*, 2018, pp. 11–103.

[21] W. Shi *et al.*, "Real-time single image and video super-resolution using an efficient sub-pixel convolutional neural network," in *Proc. IEEE Conf. Comput. Vis. Pattern Recognit. (CVPR)*, Jun. 2016, pp. 1874–1883.

[22] J. Meng *et al.*, "High-speed, sparse-sampling three-dimensional photoacoustic computed tomography *in vivo* based on principal component analysis," *J. Biomed. Opt.*, vol. 21, no. 7, 2016, Art. no. 076007.

[23] B. M. Larney, J. Rebling, Z. Chen, X. L. Deán-Ben, S. Gottschalk, and D. Razansky, "Uniform light delivery in volumetric optoacoustic tomography," *J. Biophoton.*, vol. 12, no. 6, 2019, Art. no. e201800387.

[24] X. L. Deán-Ben and D. Razansky, "Optoacoustic image formation approaches—A clinical perspective," *Phys. Med. Biol.*, vol. 64, no. 18, p. 18TR01, 2019.

[25] M. Xu and L. V. Wang, "Universal back-projection algorithm for photoacoustic computed tomography," *Phys. Rev. E, Stat. Phys. Plasmas Fluids Relat. Interdiscip. Top.*, vol. 71, no. 1, Jan. 2005, Art. no. 016706.

[26] A. Ozbek, X. L. Deán-Ben, and D. Razansky, "Realtime parallel back-projection algorithm for three-dimensional optoacoustic imaging devices," in *Proc. Eur. Conf. Biomed. Opt.*, 2013, Art. no. 88000I.

[27] Y. Li *et al.*, "Snapshot photoacoustic topography through an ergodic relay for high-throughput imaging of optical absorption," *Nature Photon.*, vol. 14, pp. 164–170, Jan. 2020.

[28] X. L. Deán-Ben, A. Özbek, H. López-Schier, and D. Razansky, "Acoustic scattering mediated single detector optoacoustic tomography," *Phys. Rev. Lett.*, vol. 123, no. 17, Oct. 2019, Art. no. 174301.

[29] J. Tang *et al.*, "Noninvasive high-speed photoacoustic tomography of cerebral hemodynamics in awake-moving rats," *J. Cerebral Blood Flow Metabolism*, vol. 35, no. 8, pp. 1224–1232, Aug. 2015.

[30] J. Yao *et al.*, "High-speed label-free functional photoacoustic microscopy of mouse brain in action," *Nature Methods*, vol. 12, no. 5, p. 407, 2015.

[31] S. Gottschalk *et al.*, "Rapid volumetric optoacoustic imaging of neural dynamics across the mouse brain," *Nature Biomed. Eng.*, vol. 3, no. 5, p. 392, 2019.

[32] B. Rao, R. Zhang, L. Li, J.-Y. Shao, and L. V. Wang, "Photoacoustic imaging of voltage responses beyond the optical diffusion limit," *Sci. Rep.*, vol. 7, no. 1, Dec. 2017, Art. no. 2560.

[33] J. Zhang and N. Tansu, "Optical gain and laser characteristics of InGaN quantum wells on ternary InGaN substrates," *IEEE Photon. J.*, vol. 5, no. 2, Apr. 2013, Art. no. 2600111.

[34] S. Azodolmolky *et al.*, "Experimental demonstration of an impairment aware network planning and operation tool for transparent/translucent optical networks," *J. Lightw. Technol.*, vol. 29, no. 4, pp. 439–448, Feb. 15, 2011.